Click to view slide presentation (5.74 MB)

The Use of CSEM and the Exploration Challenges in the Vøring Basin (Norwegian Sea)*

Aristofanis Stefatos[2], Alexander Vereshagin[1], George Vardoulias[2], Stein Kjetil Helle[2], Torolf Wedberg[2], and Susanne Sperrevik[2]

Search and Discovery Article #11040 (2018)**
Posted March 19, 2018

*Adapted from extended abstract prepared in conjunction with oral presentation given at AAPG/SEG 2017 International Conference and Exhibition, London, England, October 15-18, 2017
**Datapages © 2018 Serial rights given by author. For all other rights contact author directly.

[1]M Vest Energy, Bergen, Norway (alexandre@mvestenergy.no)
[2]M Vest Energy, Bergen, Norway

Abstract

Within a period of six months, from the end of 2014 and into June 2015, four consecutive discoveries were made in the deep water Vøring Basin in the Norwegian Sea. These wells add to a total of eight wells drilled on structural highs along an axis extending from the Vema dome to the south up to the Nyk High to the north. Seven out of the eight wells have been gas discoveries, while one of them has in addition proven a 4-meter-thick oil leg under the gas (Senfrid North, 6706/12-2). Several 2D CSEM survey lines were acquired in the area in 2003, 2007 and 2010, testing nine different structural highs, of which four have been tested with drilling. A review of the CSEM data shows a 100% correlation between our interpretations and the drilling results, with two out of the four interpretations made prior to drilling the Ivory (6707/10-3s, 2014) and the Gymir (6706/11-2, 2015) gas discoveries. The other two true interpretations are the Vema (6706/11-1, 2001) dry well and the Luva (6707/10-1, 1997) gas discovery. Following the recent successful drilling results, two 3D CSEM surveys were designed and acquired for the first time in the area, to overcome the CSEM imaging challenges over some of the yet undrilled but still appearing resistive structural highs. Constraining the depth of deeper resolved anomalies, separating between tentatively stacked resistors, steeply dipping geology, and shallow resistivity variations, are the key reasons why 3D data are needed. South of the Vema dry well and the Gymir gas discovery, there is a CSEM anomaly corresponding to the seismically mapped prospect at Upper Cretaceous (Nise Formation) level within the recently awarded exploration license PL897 that stands out. This is as a structural trap associated with a very poor seismic response and a localized resistivity anomaly. The overlying, remobilized ooze layers distort the seismic imaging, and this makes the CSEM data the key information for the de-risking the prospect. The CSEM imaging challenges in the area will be discussed further together with the nicely fitting resistivity anomaly that is attributed to the presence of hydrocarbons.

CSEM Surveys in the Vøring Area

In between 2003 and 2015 multiple 2D and 3D CSEM surveys were acquired in the Vøring Basin, Norwegian Sea (Figure 1). The authors were actively involved in design, processing, and analysis of most of these surveys. Recently, from the end of 2014 and into June 2015, four consecutive discoveries were made in this basin. These wells add to a total of 8 wells drilled on structural highs (targeting Cretaceous fault bounded three-way dip closures) along an axis extending from the Vema dome to the south up to the Nyk High to the north. Seven out of the eight wells have been gas discoveries, while one of them has in addition proven a 4-meter-thick oil leg under the gas (Senfrid North, 6706/12-2). Further to the west, in the outer Vøring Basin, one additional well (Stordal 6705/7-1) was drilled in 2017, over a similar structural high. The well tested upper Cretaceous sands that were proven to be water wet. A review of the CSEM data shows a 100% correlation between our interpretations and the drilling results, with three out of five interpretations made prior to drilling are the Ivory (6707/10-3s, 2014), Gymir (6706/11-2, 2015) gas discoveries and the Stordal (6705/7-1) water wet reservoir. The other two correct interpretations are the Vema true negative (6706/11-1, 2001) dry well, and the Luva true positive (6707/10-1, 1997) gas discovery. The pre-drill interpretation of the most recent Stordal (6705/7-1, 2017) dry well is not discussed in this article due to confidentiality restrictions.

The CSEM data processing and analysis referred to in this article was performed over many years and employed multiple algorithms and software packages. The standard practice for the applied workflows was that all of the results have been verified by at least two algorithms. The list of algorithms/software includes (but not limited to): Rocksource Discover; Optimized integral equation, full 3D anisotropic code, courtesy of GeoContrast AS; MARE2DEM (see Constable et al., 1987; and Key and Oval, 2011) with interface provided by BlueGreen Geophysics and cloud implementation by M Vest Energy; 3D modeling and inversion courtesy of EMGS; WinGLink and IEM by Schlumberger; Proprietary software packages developed by M Vest Energy.

The Need for Apriori Information

The first CSEM lines in the area were collected by EMGS in 2003 to test the response from the Luva discovery (6707/10-1, 1997) (today part of the Aasta Hansteen field development). Although the discovery is of considerable size (circa 80 mmboe of gas), no significant EM anomaly was initially resolved. To resolve the target, a guided inversion workflow was successfully applied in 2007 for Nagrind04 CSEM line (see Figure 1), which demonstrated that CSEM technology can be successfully applied in the area *(*Hesthammer et al., 2007*)*. The main idea was to create an "apriori" model, closely resembling the resistivity profile expected in the survey area. This model was input to CSEM inversions where the deviation from the starting model was weighted/penalized in the inversion functional (see also Myer et al., 2015 and references therein). Contrary to inversion without geological input, this scenario resolved the target (Figure 2). It was also demonstrated that the model does not have to be very precise to resolve the target, therefore such analysis is also possible to carry before the actual drilling.

Inspired by these results, several 2D CSEM surveys were acquired in the area during 2007-2010 CSEM reconnaissance campaigns (see, e.g., Sperrevik et al., 2010). These campaigns mapped many structures in the area. Some of the structures are associated with high resistivity anomalies while others do not appear to be as resistive. Three of them were drilled since then. The first one is the Ivory gas discovery drilled in December 2014 (Stefatos et al., 2015a). The second is the Gymir gas discovery drilled in May 2015 (Stefatos et al., 2015b). The third well which was not associated with any resistive anomaly was the Stordal drilled in April 2017 and turned out water wet.

After the first reconnaissance 2D CSEM surveys, four multiclient surveys were acquired by EMGS: NSMCA (2010), MCPL705 (2014), MCPL528 (2015), MCPL763 (2015) (for locations see Figure 1). However, it is worth noting that all three drilling decisions were made at a time when only 2D CSEM data were available. Some preliminary results from MCPL763 survey will be shortly discussed later.

The Unforeseen Complexity of Stacked Resistive Bodies

The Ivory discovery is located in the Nyk High area, at water depth of about 1400 m (see Figure 1). Since the discovery of Luva, the Ivory neighboring structure had attracted the interest of exploration companies. However, level flat spots and AVO anomalies of limited extent at Upper Cretaceous Nise Formation pointed towards limited volumes of trapped gas. Deeper, the Upper Cretaceous Kvitnos sands do not show clear flat spots or AVO fluid effects and this prevented drill decisions from being made. Seismic imaging problems, such as multiples, fault shadow effects and speculated seismic velocity changes across the faulting, meant that the interpretation of the seismic data could not be conclusive. The conclusive interpretation of the seismic data was further hindered by synthetic seismic modeling suggesting that slightly worst quality reservoir sands filled with oil instead of gas would not return clear flat spots or AVO effects. To improve the de-risking of the Ivory prospect 2D CSEM surveys were initially collected over the structure (IVOR01, 02; EMGS 2007) but also over two neighboring, similar structures West of Ivory and North of Luva (TOUR01; EMGS 2007).

The analysis of both IVRO01 and 02 survey lines revealed a strong anomaly over the Ivory prospect. The analysis was performed together with the adjacent survey (TOUR01, Figure 1), which demonstrated that neighboring similar structures (Nephrite and Tourmaline) are not as resistive (Figure 3). The tentative interpretation of hydrocarbons over Ivory and absence of hydrocarbons over Nephrite and Tourmaline not only explained the CSEM data but are also consistent with hydrocarbon migration modelling results that suggested Nephrite and Tourmaline lied on migration shadow zone.

Prior to drilling Ivory there were conflicting views and interpretations of the CSEM data, with some arguing that the sensitivity of the survey to the primary Kvitnos target was such that the data should not be used for de-risking. Our interpretation of the CSEM data was largely based on the fact that the recorded EM responses over the Ivory structure could not be explained without significant deviations from a well constrained anisotropic background resistivity model. In order to disregard the data, we thought that first the excessive resistivity should be explained without the introducing hydrocarbons in the structure.

In our view, the possibility of oil could not be ruled out (a theory which was soon after confirmed by the oil leg discovered in the Snefrid North well) and this increased the number of the plausible models that could fit the CSEM measurements. The final interpretation of the 2D CSEM data included three scenarios: i) a relatively thin but aerially extensive oil leg under the small gas pockets at the crests of Top Nise, ii) a big gas accumulation at Kvtinos and the same gas pockets at Top Nise, iii) increased resistivity of the geology from Top Kvitnos and lower due to a yet unknown reason (Stefatos et al., 2014 and Stefatos et al., 2015a) (Figure 3). Several factors contributed to the final interpretation not being more precise. The most important were: (a) the lack of 3D data, (b) the presence of overlapping prospects and the particular geological setting that among other included shallow resistors, and (c) the suboptimal positioning of the survey line relative to the structure (CSEM survey designed on 2D seismic prior to acquiring 3D seismic).

While the burial depths of potential Springar and Nise prospects are relatively small (less than 1.5 km), the main target at Kvitnos level is relatively deep (around 2 km below mudline in the CSEM line location) and thus presented challenges for CSEM detection and especially, delineation (2007 data vintage). Figure 4 highlights the uncertainty: the majority of unconstrained inversions were indicating resistor at Kvitnos level, while a subset of apriori (guided) inversions have shown weak indications of Nise resistors. Similar results were also obtained using the Schlumberger 3D inversion (including a parallel survey line with azimuthal receivers) and later EMGS 3D inversion algorithms.

The prospect was drilled in late 2014, with the well (6707/10-3 S) that encountered 12 meters of gas in Kvitnos and confirmed more than 200 m gas column. Preliminary estimates of the discovery size suggest recoverable gas between 2 and 8 GSm3. Although the actual discovered volumes are still not well constrained, the size of the discovery was less than what it was predicted for the Kvitnos gas case. This was due to a relative thick free water zone under the discovery that is saturated by low salinity water and thus effectively increasing the resistivity of the water wet sands beyond what was expected (Stefatos et al., 2015a and Stefatos et al., 2015b).

To help delineate the discovery, and examine the remaining potential of the area we helped to design and prefunded a new 3D CSEM survey (multiclient) that was shot in 2015 (MCPL528, see Figure 1). The data analysis of the 3D survey is currently on-going.

Tentative Challenges from the Shallow Geology

In the Vema dome area, south west of Nyk High, the Gymir gas discovery was drilled in 2015 in between the 6706/11-1 dry well (drilled in 1997) and the Roald Rygg gas discovery (6706/12-3 well, drilled also in 2015, prior to Gymir). Contrary to the neighboring Roald Rygg, the Gymir discovery is well defined by a clear seismic flat spot and a class 3 AVO response. The Gymir discovery is covered by VEMA01 survey (EMGS 2010), which also goes over 6706/11-1 well (Figure 1). To ensure that the observed direct hydrocarbon indicators (DHI's) on the seismic were not due to low saturation gas, this CSEM line was utilized. A potential collateral benefit of the analysis is a better assessment of our ability to confidently map and delineate with CSEM the poorly imaged seismic Roald Rygg discovery.

CSEM feasibility studies have shown that even the smallest Cretaceous prospects of commercial value should be detectable by CSEM in this area. The Gymir burial depth is relatively small (approximately 1.1 km below mud line), and clearly within the typical CSEM detectability window. A standard CSEM analysis of VEMA01 data, however, did not demonstrate a clear evidence of resistivity anomaly in the prospect location. The absence of a clearly resolved resistivity anomaly over Gymir could mean that the anticipated chances of success should drop dramatically (Hesthammer et al., 2010), and that is why for a drill decision it was essential to verify whether the CSEM data support a hydrocarbon positive interpretation.

As seen from Figure 5B, the unconstrained (no apriori information) anisotropic 2.5D inversion does not resolve a clear anomaly in Gymir. What is however easy to see, is the overall ρ_V (vertical resistivity component) increase in Brygge and Springar levels – just above the prospect. Further, there are resistivity anomalies above Top Brygge, partially overlapping with lateral location of the prospect. Thus, one can suspect that there are multiple ("stacked") resistors which inversions fail to resolve without additional guidance/regularization. Preliminary feasibility modeling also demonstrated such inversion behavior in this background pattern.

By analogy with Luva and Ivory it was decided to incorporate geological information by building a starting (guiding) anisotropic resistivity model for the background. The "apriori" model (Figure 5A) was built on the basis of a well calibrated, regional resistivity study, and then further fine-tuned by the resistivity log from the recently drilled 6706/12-3 (Roald Rygg) well, located 8 km to the East (Figure 1). Since the conventional well logs normally underestimate the actual vertical resistivity (see, e.g., Wedberg et al., 2017), the additional studies were performed to estimate ρ_V. The result of corresponding guided inversion is shown in the Figure 5C, where one can see that the resistivity enhancement in the target location became more pronounced (numerical fit around target location has also improved). Further, by applying shallow resistivity constraints and relaxing the penalties for deeper layers, the target resistor was better localized, while numerical fit remained the same (e.g., result in Figure 5D).

The analysis of VEMA01 survey was completed early 2015 (Stefatos et al., 2015b) and Gymir was drilled in the summer 2015 (6706/11-2 Wildcat well) and became a gas discovery.

The study revealed that the shallow siliciclastic ooze bodies could exhibit a wide range of resistivities varying from being conductive to being more resistive than the surrounding shallow sediments (ρ_V). Underneath the base of the ooze the Paleogene stratigraphy appears as a relatively uniform low resistivity interval. When the vertical distance between the relatively resistive ooze and the high resistivity hydrocarbon-filled Cretaceous sands is small (thin Paleogene) then the CSEM imaging through inversions is challenged. The analysis has demonstrated that although the shallow ooze bodies could potentially create complications for CSEM imaging, the problem however is likely less severe as for the seismic imaging. Careful well analysis and advanced CSEM inversion scenarios can help to image the prospect. Moreover, CSEM value is substantially increased in such cases, as seismic imaging reliability is compromised. The study illustrated again the main complication related to non-uniqueness of CSEM inversion result. The three inversion results in Figure 5 have very similar numerical fit: about 3% standard deviation, which can be considered very good compared to the variations of the response and the noise estimates. At the same time, only the guided inversions with seismic input (Figure 5C and Figure 5D) support HC-positive interpretation. Thus, it is essential to supply the geology information (Figure 5C) and, perhaps, constraints to the inversion algorithm (Figure 5D). In addition to it, most of 2.5D inversion scenarios have shown sensitivity to underlying 3D structures which, again, contributes to non-uniqueness of the solution. A 3D CSEM survey could have been much more efficient in mapping the prospect. These results contributed to the survey design of later shot 3D surveys MCPL528 and MCPL763. Some preliminary results from the analysis of the latter are discussed in the next section.

Pushing the Envelope Deeper

About 15 km south of Gymir, the Karius prospect (also referred to as Harald) is another Upper Cretaceous (Nise1 Formation) fault-bounded three-way-dip closure. The prospect is buried at approximately 1950 m below the mud line on the southern flank of the Vema dome (Vøring Basin), at water depth of about 1150 m. The expected fill levels (P90 to P10) correspond to an area between 6.2 km^2 and 15.4 km^2 with hydrocarbon column heights between 160 m and 220 m. The primary hydrocarbon phase is gas with many analogue discoveries nearby (Luva, Haklang, Snefrid South, as well as the recent Snefrid North, Roald Rygg, and Gymir).

As in the Gymir case, Karius is overlain by layers of insitu and remobilized siliceous ooze, but in this case the remobilized ooze bodies cover significantly larger area (see Figure 6). These are low density and low seismic velocity layers that appear as irregularly shaped lenses of

varying thickness and extent. The interfaces between the remobilized ooze and the overlying and underlying sediments are thus characterized by high acoustic impedance contrast that results in scattering and absorption of the seismic waves. This creates significant challenges and limitations to the seismic imaging. In particular, conventional seismic surveys and conventional processing does not allow reliable seismic amplitude preservation. It is thus difficult to run seismic DHI analyses, and consequently drill decisions are likely of higher risk. To assist the de-risking of Karius old and new CSEM data have been utilized.

A 2D CSEM survey line from 2007 runs over the long axis of the Karius prospect (Figure 1 and Figure 6, PERI01 survey). Due to the relative deep burial depth of Karius (1950 m below the mudline) this survey utilized a narrow band frequency source (0.25 Hz square waveform) to ensure the detection of a potential deep target. However, this frequency content is not sufficient for detailed delineation studies, particularly when the resistivity varies significantly also above the target. A recent feasibility study for Karius prospect demonstrated that Karius is detectable if the fill is equal to or above the P50 levels, although the inversion may need geological input to resolve the target. Indeed, in good accordance with modeling results, the attribute analysis of PERI01 data shows a far offset anomaly above 25%.

The unconstrained inversion of PERI01 dataset assuming minimum 3% standard error (and independent receiver noise floors; error handling in MARE2DEM algorithm is described in, e.g., Myer et al., 2012 and Myer et al., 2015) is shown in Figure 7A. A relatively small anomaly in the prospect location is resolved, however this anomaly is too weak to allow a reliable interpretation. By tightening the minimum error to approximately 1% (even though this could lead to data over-fitting) it is possible to obtain more significant resistivity increase in the prospect location (Figure 7B). Nevertheless, the anomaly is still not well localized and its fit to the prospect extent is ambiguous. Building on the experience gained from the previous cases in the area, a workflow of guided inversions was then applied.

The anisotropic background resistivity model for the area is now well constrained thanks to the extensive database available and the recent drilling (Ivory, Roald Rygg, Gymir, and Stordal wells) that proved the accuracy of the model. This resistivity model, fine-tuned to the nearest wells and neighboring surveys was used as apriori (guiding) model for the inversions (Figure 8). The guided inversion analysis was performed in many steps, by varying inversion parameters/weights and noise model constraints. The inversion workflow was repeated on the re-processed version of the data, where the reprocessing allowed to reduce minimal error to 2%.

As shown in Figure 8, the guided inversions confirm increased resistivity over the Karius prospect. A sharp and highly reliable termination of the increased resistivity occurs repeatedly where Karius terminates against the main bounding fault. However, all inversions in the figure show the resistive anomaly extending southwest outside of the Karius prospect (P_{Max}) outlines. Without constraints (“guidance only”) the Karius anomaly appears weaker and less localized (Figure 8B), while an increased resistivity "cloud" develops above and around Top Springar. When the resistivity cloud is removed from Springar by applying well constraints (Figure 8C and Figure 8D), the extra resistivity develops above Top Kai, and/or, below Top Nise mainly towards the southwest. We therefore conclude that more resistivity southwest of Karius is needed to fit the data, but it is unclear which depth level this resistivity should belong to, since all inversions converge to similar numerical data fit. This could be due to various reasons like: (a) inversion artefact due to an unresolved resistive body, (b) Karius closure extending further to the southwest but not visible due to depth conversion uncertainty, (c) noise in the data. It is worth noting that similar results were obtained by an independent external study utilizing the Schlumberger 2.5D inversion code.

Since the data is 2D, it is impossible to compare the fit to closure on other directions. Similarly, it is impossible to rule out the possibility of a 3D side effect, where a resistive body not directly under the survey line contributes to the resolved anomaly.

A new 3D survey (MCPL763, see Figure 1 and Figure 6) was designed and shot in July 2015 as multiclient data. Apart from standard (staggered) receiver grid, it included an additional towline and infill receivers running over the long axis of the Karius prospect, close to the PERI01 survey line. This line makes it possible to repeat the 2.5D inversion workflows (fine-tuned on PERI01) as a secondary and independent test to the 3D inversion, and also for a direct comparison to the earlier results. To improve the resolution, a source waveform with a rich selection of harmonics was used. The overall data quality achieved is considered good with less than 3% noisy channels, however light noise is present at 40% receivers (reported due to seabed water currents).

The analysis of new 3D data involves multiple scenarios of 2.5D and 3D inversions and is not yet finalized. Some preliminary conclusions from the analysis of the 3D data include: (a) a confirmation of the resistivity anomaly over the Karius prospect, (b) additional resistivity anomalies, (c) the resistive remobilized ooze is confirmed and confidently mapped by inversion, (d) volcanic intrusions (including sills) mapped on seismic did not return resistive responses, which reduces the risk of "seismically invisible" and resistive sills being present over the prospect area.

Sand intervals with low salinity pore water that increase the formation resistivity have been observed in the 6707/10-3S well at the Kvitnos Formation level. However, increased resistivity values of similar level have not been encountered in the water zones in any of the surrounding wells *above* Kvitnos. Still, a low salinity water filled reservoir (Nise1) at Karius cannot be excluded and could potentially explain to some degree the observed anomaly. To this date, no other challenging resistive features that are likely to create a false-positive response at the prospect location have been identified. Still, misinterpretation of stacked resistive responses is possible although less likely (e.g., low hydrocarbon saturation in Karius, and interference from shallower or deeper anomalies).

Conclusions

We have presented a short overview of some of the CSEM work performed by the authors over the last 10 years in the Vøring Basin of the Norwegian Sea. Emphasis is put on recent discoveries in the area and on the steps necessary to effectively de-risk such prospects. In particular, it is demonstrated that careful analysis of the background used in inversion workflow is necessary, and a relatively accurate background resistivity model, with lighter or heavier guidance, is essential for all algorithms tested in order to improve the mapping of the made discoveries. The relative weighting of the guidance and the need of constrains is subject to a number of parameters like (a) the presence of shallow resistive bodies and their vertical distance from the target, (b) the thickness of the Paleogene interval, (c) the size and resistivity of the target relatively to its burial depth, and (d) the possibility of stacked resistive bodies. Figure 9 gives a schematic summary for the cases discussed in this abstract. To our knowledge, there has been no case of false negative interpretations (discoveries constituting feasible targets that have not been detected with CSEM).

A yet untested prospect is presented together with a discussion of the current results from the analysis of the CSEM data. Although the work is still on-going, it is very likely that the CSEM data will allow to reduce the prospect risk.

Acknowledgements

We are grateful to David Myer from BlueGreen Geophysics and Efthymios Tartaras and his colleagues at the Integrated Electromagnetic Center of Excellence in Milan for their collaboration on analysis of the IVOR01-02 surveys. We are grateful to EMGS for constant collaboration on design and analysis of multiple CSEM surveys during the last 10 years. We are grateful to many of our present and former colleagues in Rocksource, Emergy Exploration and Atlantic Petroleum for valuable discussions and input during all these years.

References Cited

Boulaenko, M., J. Hesthammer, A. Vereshagin, P. Gelting, R. Davies, and T. Wedberg, 2007, Marine CSEM Technology - The Luva Case: Houston Geological Society Bulletin, December 2007, p. 23-43.

Constable, S., R.L. Parker, and C.G. Constable, 1987, Occam's Inversion: A Practical Algorithm for Generating Smooth Models from Electromagnetic Sounding Data: Geophysics, v. 52/3, p. 289-300.

Davydycheva, S., and M.A. Frenkel, 2013, The Impact of 3D Tilted Resistivity Anisotropy on Marine CSEM Measurements: The Leading Edge, v. 32/11, p. 1374-1381.

Fanavoll, S., J. Hesthammer, J.E. Danielsen, and A. Stefatos, 2010, Controlled Source Electromagnetic Technology and Hydrocarbon Exploration Efficiency: First Break, v. 28, p. 61-69;

Hesthammer, J., A. Stefatos, and S. Sperrevik, 2012, CSEM Efficiency – Evaluation of Recent Drilling Results: First Break, v. 30, p. 47-55.

Hesthammer, J., S. Fanavoll, A. Stefatos, J.E. Danielsen, and M. Boulaenko, 2010, CSEM Performance in Light of Well Results: The Leading Edge, v. 29/1, p. 34-41.

Hesthammer, J., A. Verechtchaguine, P. Gelting, M. Boulaenko, R. Davies, and T. Wedberg, 2007, The Luva Gas Field: Detailed Analyses Reveal Subtle CSEM Anomaly: GEO ExPro, v. 4, p. 52-58.

Jaysaval, P., D.V. Shantsev, S. de la Kethulle de Ryhove, and T. Bratteland, 2016, Fully Anisotropic 3-D EM Modelling on a Lebedev Grid with a Multigrid Pre-Conditioner: Geophysical Journal International, v. 207/3, p. 1554-1572.

Key, K., and J. Ovall, 2011, A Parallel Goal-Oriented Adaptive Finite Element Method for 2.5-D Electromagnetic Modelling: Geophysical Journal International, v. 186, p. 137-154. The latest version of the code is available via SEMC consortium: http://marineemlab.ucsd.edu/semc.html. Website accessed January 2018. Earlier versions are available free from: http://mare2dem.ucsd.edu/. Website accessed January 2018.

Li, Y., and S. Dai, 2011, Finite Element Modelling of Marine Controlled-Source Electromagnetic Responses in Two-Dimensional Dipping Anisotropic Conductivity Structures: Geophysical Journal International, v. 185, p. 622-636.

Myer, D., K. Key, and S. Constable, 2015, Marine CSEM of the Scarborough Gas Field, Part 2: 2D Inversion: Geophysics, v. 80/3, p. E187-E196.

Myer, D., S. Constable, K. Key, M.E. Glinsky, and G. Liu, 2012, Marine CSEM of the Scarborough Gas Field, Part 1: Experimental Design and Data Uncertainty: Geophysics, v. 77, p. E281-E299.

Sperrevik, S., R. Davies, A. Vereshagin, and B. Alaeimajolan, 2010, Use of CSEM in Exploration in Open Acreage - A Case Study from the 20th Licensing Round – Norway: 4th EAGE, St. Petersburg International Conference and Exhibition on Geosciences, 04 May 2010.

Stefatos, A., A. Vereshagin, and J. Hesthammer, 2014, The Ivory Discovery Presentation given at Schlumberger Integrated Electromagnetics Event Milan, 12 September 2014.

Stefatos, A., A. Vereshagin, S. Sperrevik, and J. Hesthammer, 2015a, Case Study of a CSEM True Positive-Ivory Well, Norwegian Sea: 77th EAGE Conference and Exhibition, 1-4 June 2015, Madrid, Spain. DOI: 10.3997/2214-4609.201413169

Stefatos, A., A. Vereshagin., G. Vardoulias, and L.K. Strønen, 2015b, The Vøring Basin and First Drilling Successes with CSEM Support: Hydrocarbon Habitats Seminar, Stavanger-Oslo, October 22, 2015.

Wedberg, T., A. Stefatos, and A. Vereshagin, 2017, Upscaling of Triaxial Resistivity Data Measured on the Norwegian Continental Shelf and Observations Relevant for CSEM Imaging: AAPG/SEG International Conference and Exhibition 2017, London, 15-18 October 2017.

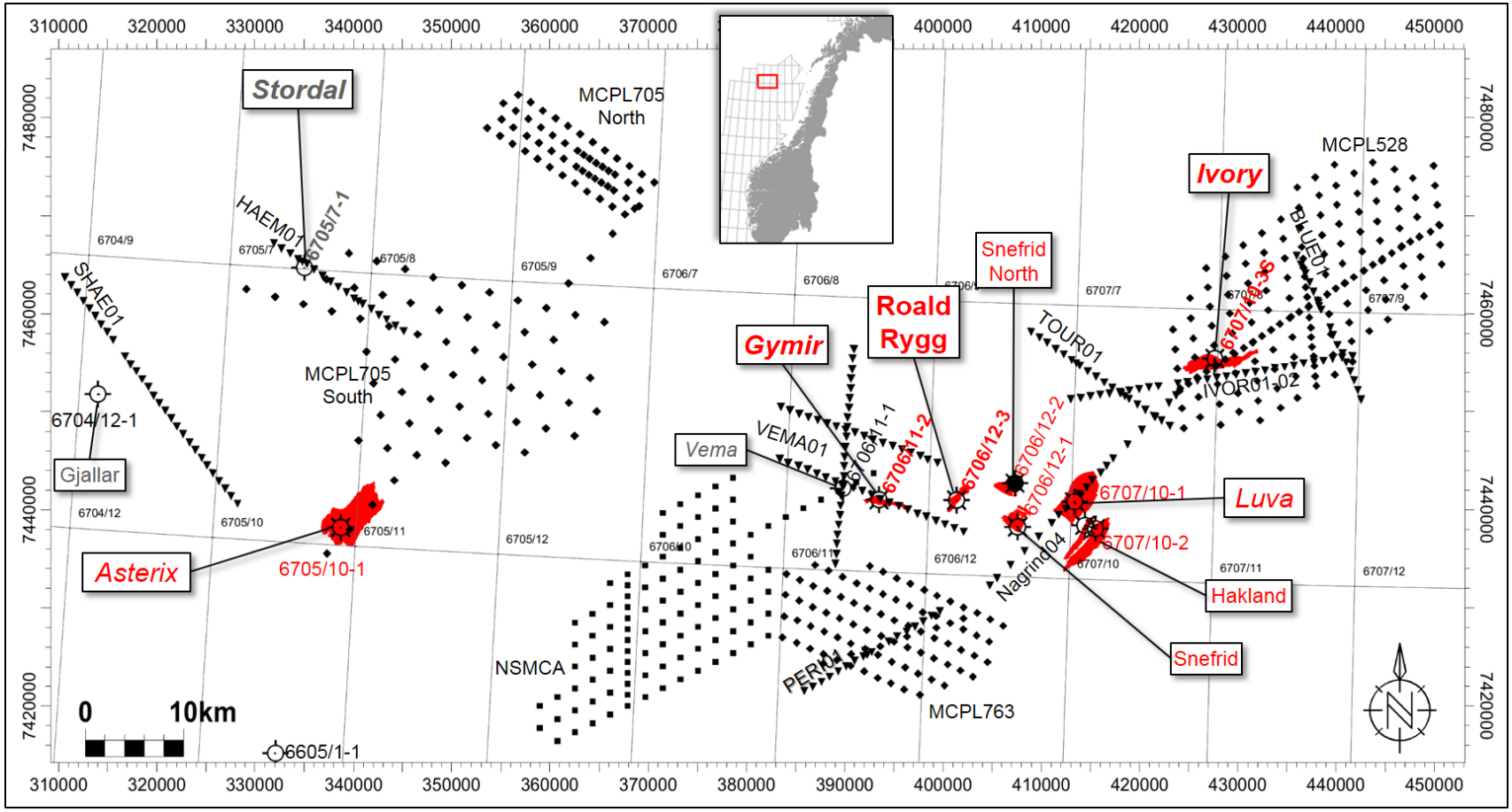

Figure 1. Acquired CSEM surveys (EMGS 2003 - 2015) in the area together with exploration wells and discoveries outlines; the 3D surveys were acquired in 2010, 2014, and 2015.

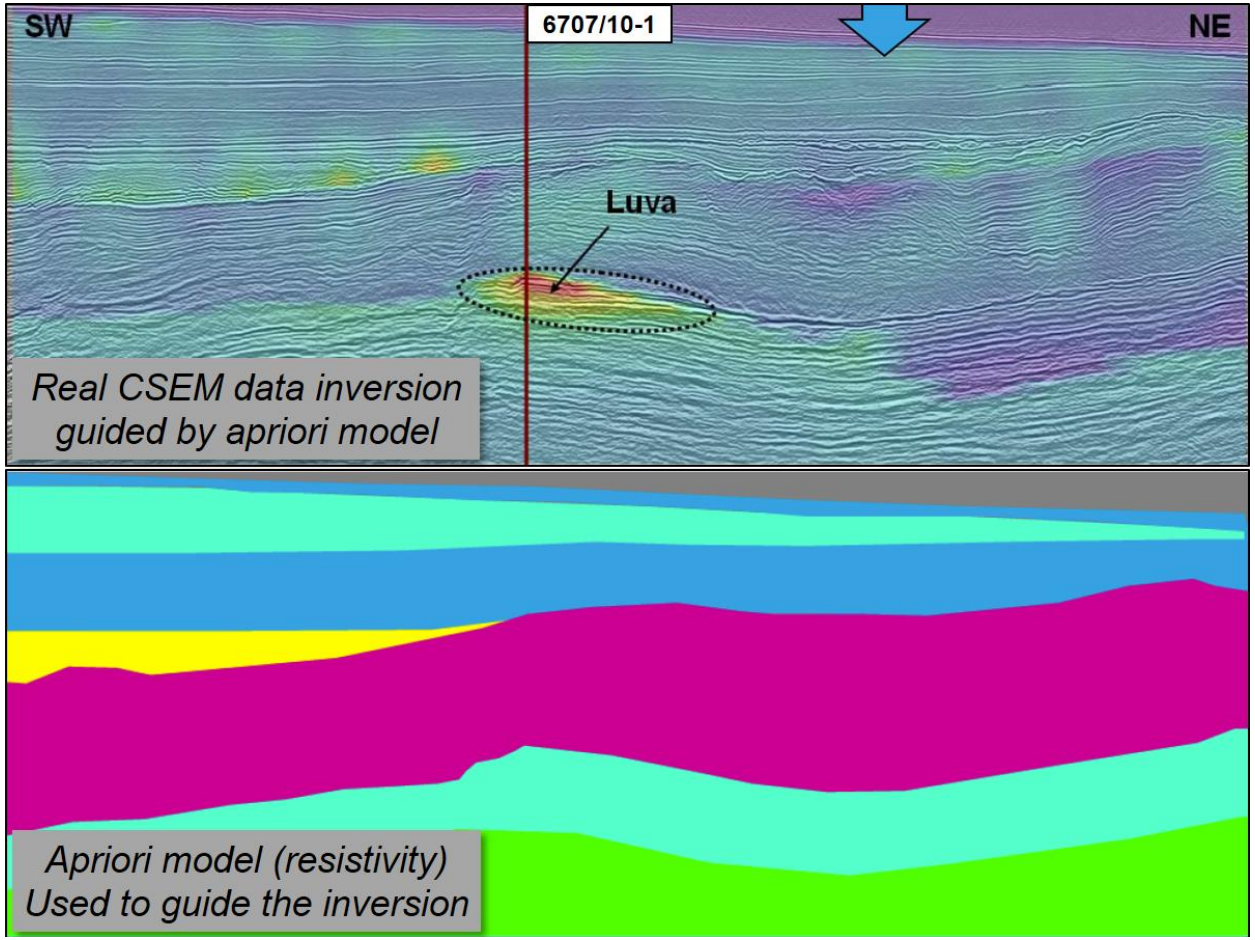

Figure 2. Guided inversion of Luva discovery (modified from Hesthammer et al., 2007).

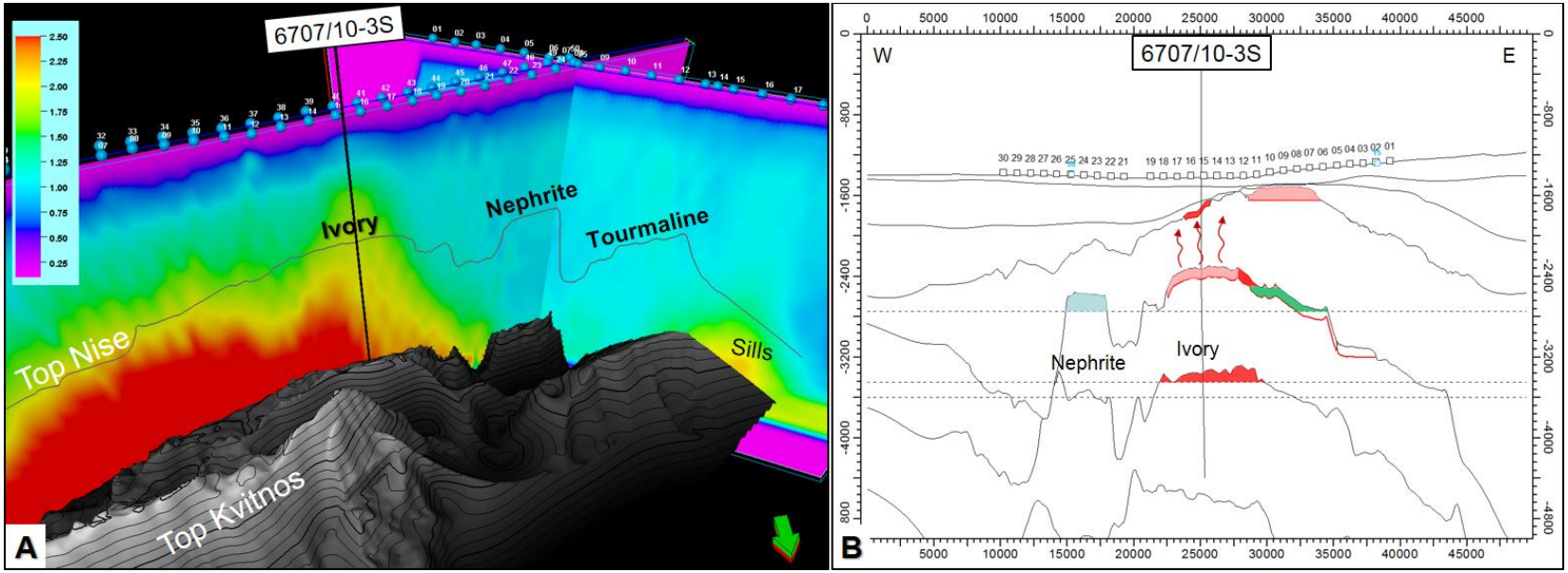

Figure 3. **A**: Anomaly over Ivory (0.75 Hz; ratio to 3D background model; modified from Stefatos et al., 2015b). **B**: Possible scenarios (modified from Stefatos et al., 2014).

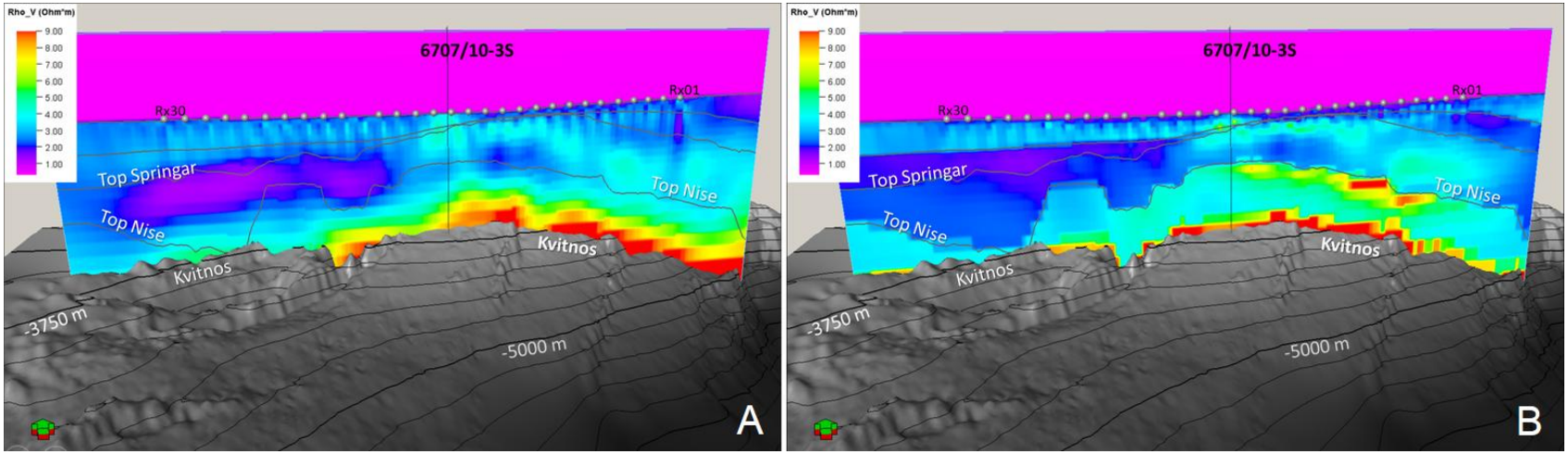

Figure 4. **A**: Unconstrained Occam inversion (MARE2DEM algorithm), ρ_V. **B**: Guided inversion (penalized for deviations from the apriori resistivity model), ρ_V. Modified from Stefatos et al., 2015a.

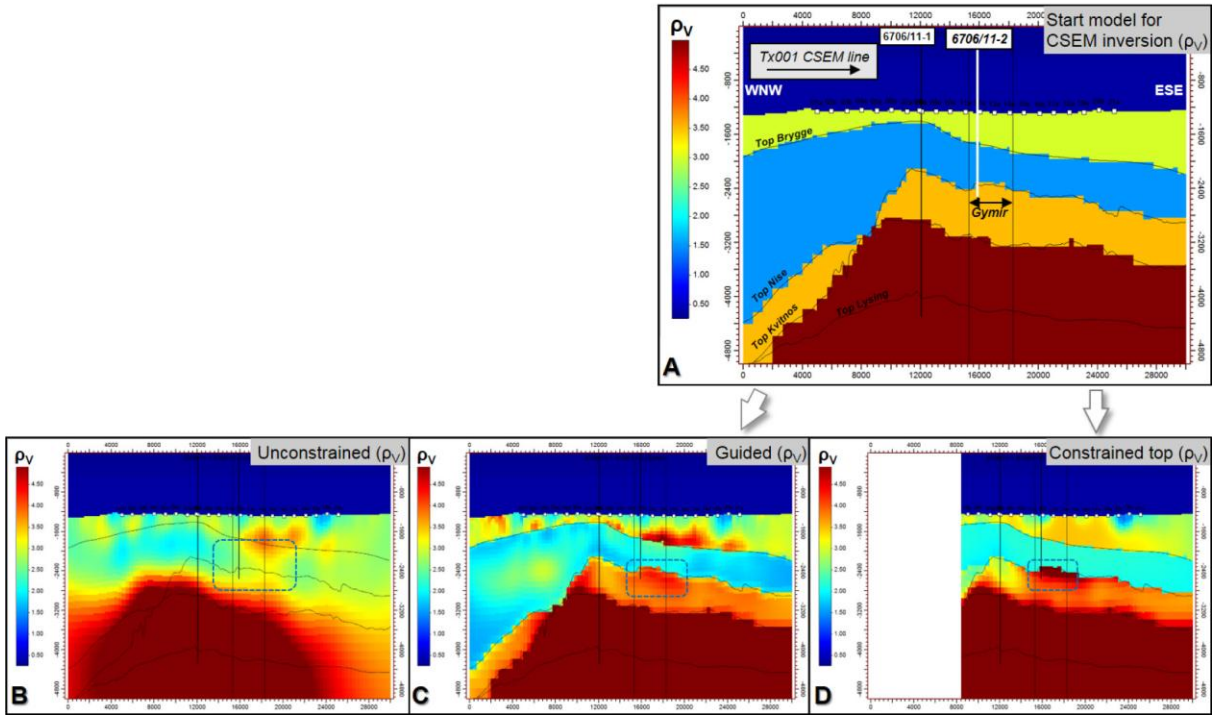

Figure 5. CSEM analysis of VEMA01 data set, ρ_V. **A**: Start model for 2.5D CSEM anisotropic inversion (MARE2DEM). The 6706/11-2 well is highlighted by white. **B**: Unconstrained inversion (MARE2DEM "Occam") - weak "resistivity column" in the lateral location of the prospect. **C**: Guided inversion - the prospect anomaly stands out from the background. **D**: Guided inversion with resistivity constrained in shallowest part - Gymir anomaly is clearly resolved. All inversions are converged to RMS = 1; error model accounts for individual receiver noise floors and about 3% error bars (standard deviation).

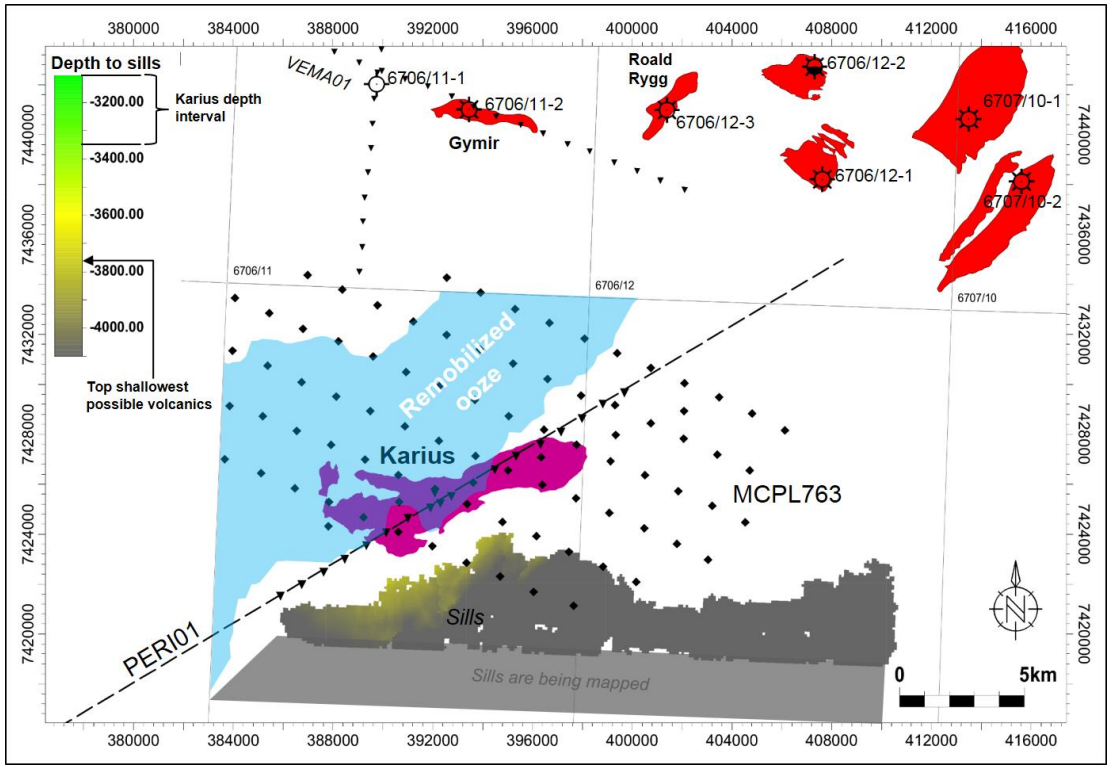

Figure 6. Overview map of the PERI01 (and MCPL763) survey area, illustrating the presence of remobilized ooze (in blue), volcanic intrusions (colored by depth) and nearby discoveries (in red). The PERI01 and MCPL763 survey footprints are shown over the Karius prospect Pmax.

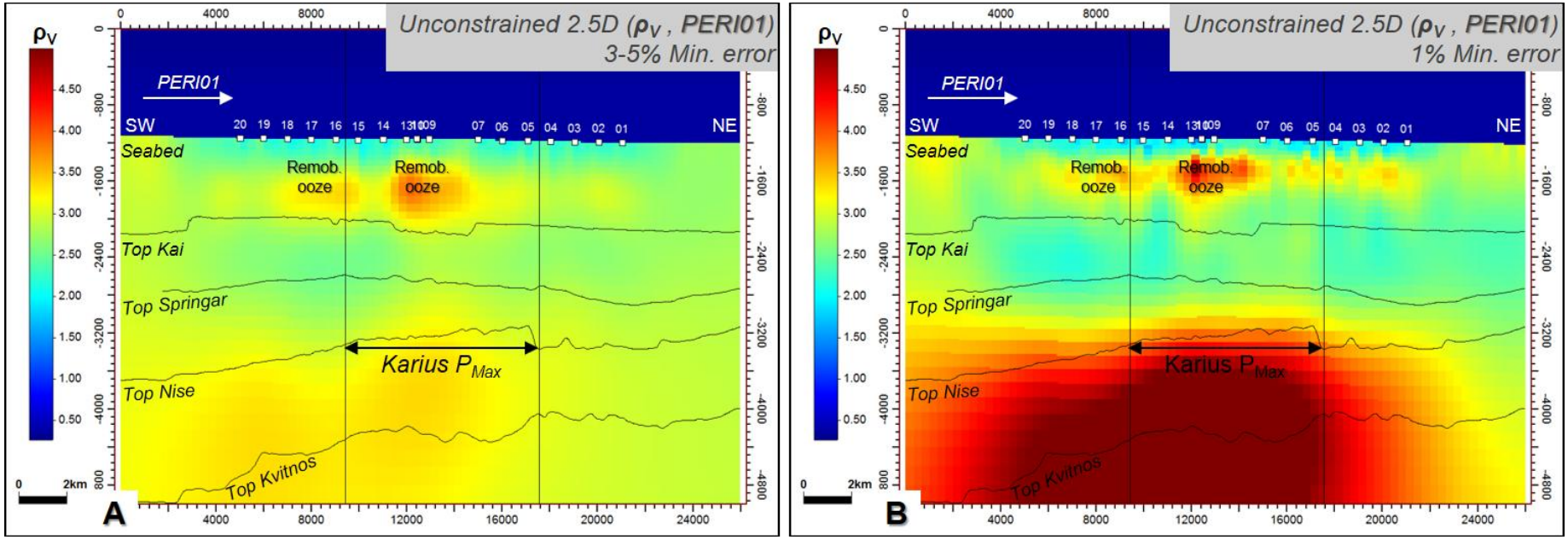

Figure 7. Unconstrained 2.5D inversion (MARE2DEM "Occam") of PERI01 data, ρ_V. **A**: Noise model with 3-5% minimum statistical error. **B**: Noise model with 1% minimum statistical error. Karius prospect max extent shown for reference.

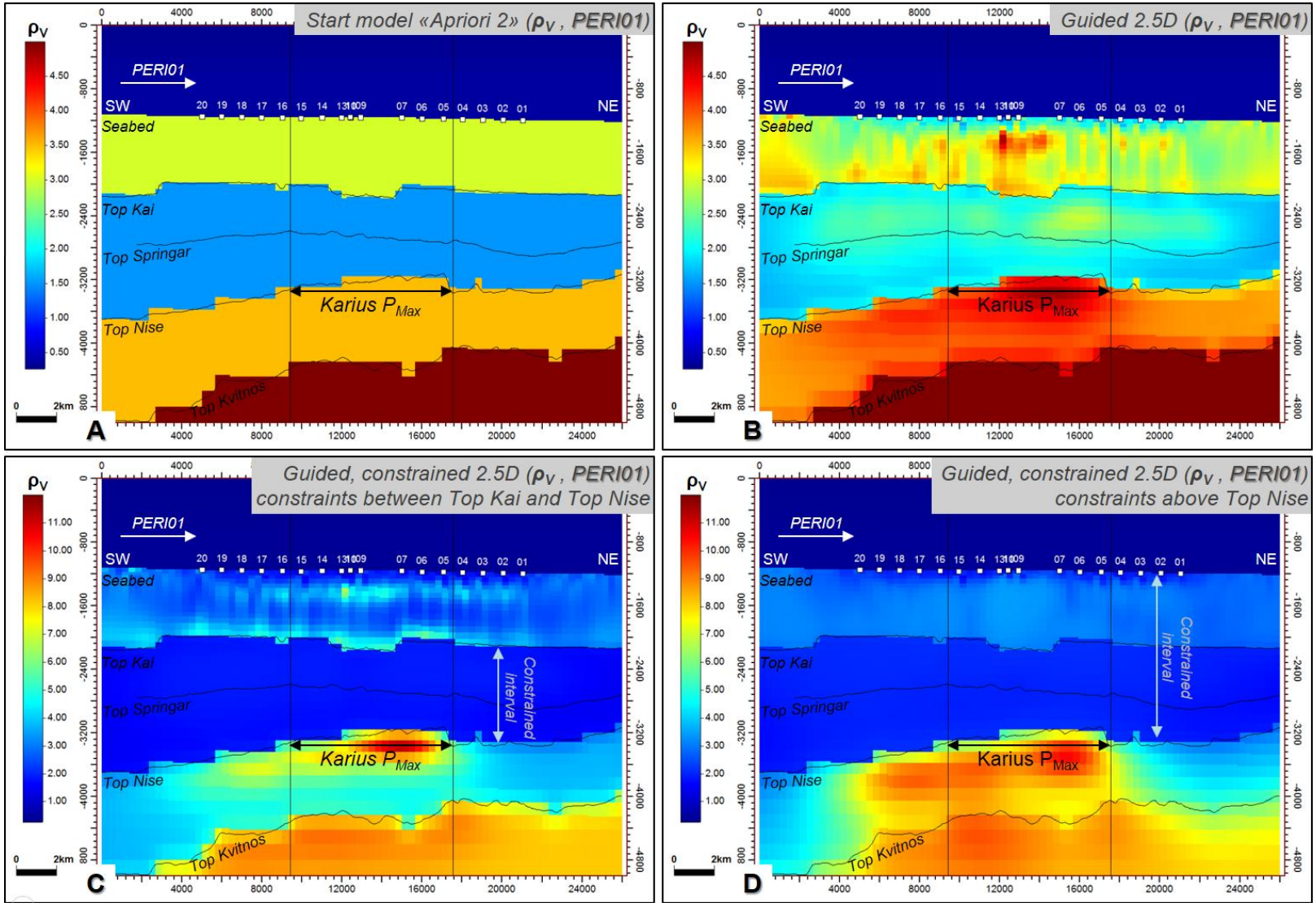

Figure 8. 2.5D inversions with the latest start model applied on PERI01 (reprocessed) dataset, ρ_V. Error model with 2% minimal error and individual receiver noise floors is applied. **A**: Starting ("apriori") model. **B**: Guided inversion. **C**: Guided inversion with additionally constrained resistivity between Top Kai and Top Nise. **D**: Guided inversion with entire subsurface constrained above Top Nise. Note that different color scales are used for first (**A, B**) and the second (**C, D**) rows of the plots. All three inversions converge well to RMS=1.

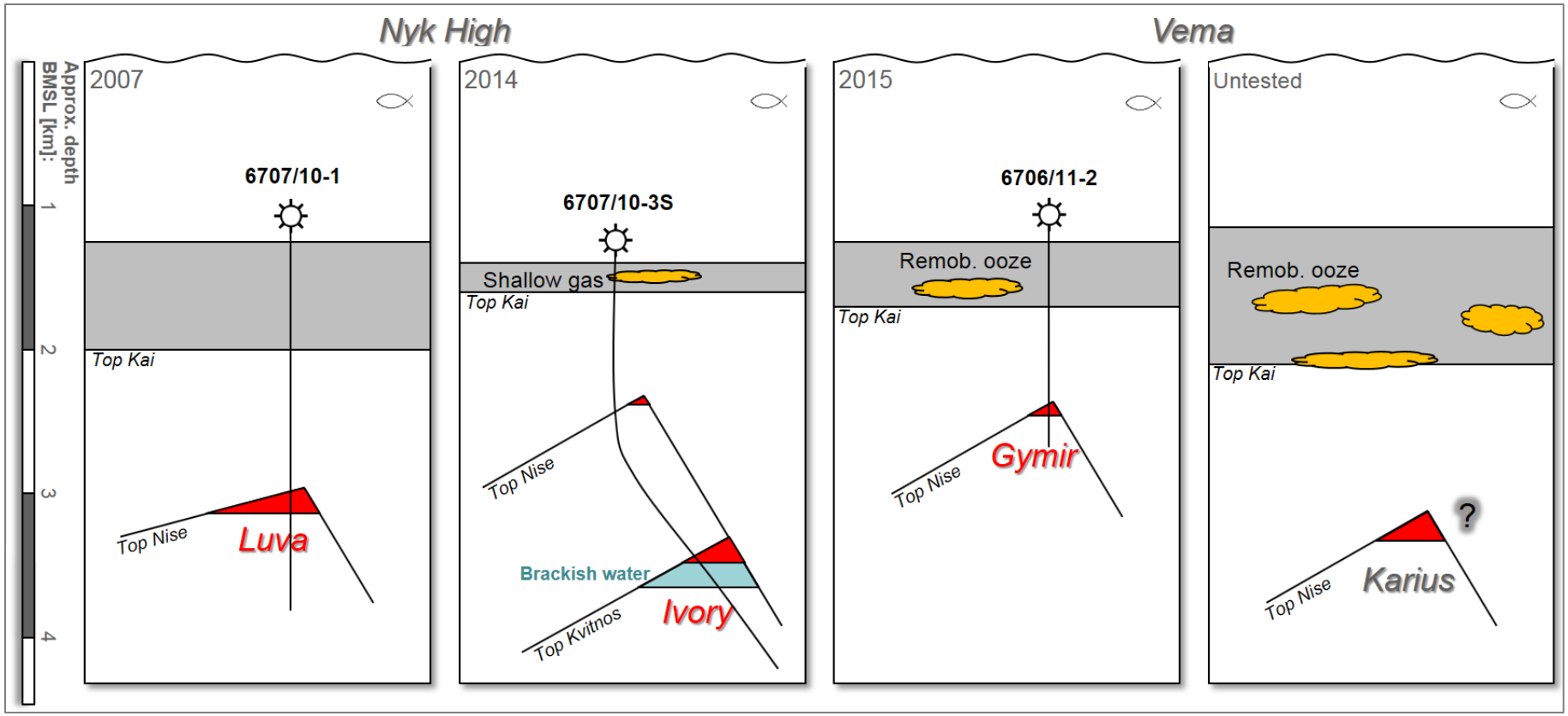

Figure 9. The four CSEM-tested prospects discussed in this abstract presented in a schematic sketch depicting key geological features. The true negative cases are not presented.